JCI insight

Cell cycle inhibitors activate hypoxia-induced DDX41-STING pathway to mediate anti-tumor immune response in liver cancer

Po Yee Wong, … , Yan Zhang, Carmen Chak Lui Wong

JCI Insight. 2024. https://doi.org/10.1172/jci.insight.170532.

Research In-Press Preview Hepatology Oncology

Graphical abstract

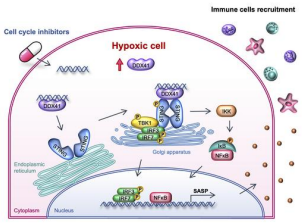

Manuscript title

Cell cycle inhibitors activate hypoxia-induced DDX41-STING pathway to mediate anti-tumor immune response in liver cancer

Authors

Po Yee Wong[1,2,3#], Cerise Yuen Ki Chan[1,2,3#], Helen Do Gai Xue[1,2,3#], Chi Ching Goh[1,2], Jacinth Wing Sum Cheu[1,2,3], Aki Pui Wah Tse[1,2], Misty Shuo Zhang[1,2,3,4], Yan Zhang[1,2,3], Carmen Chak Lui Wong[1,2,3,4,5*]

Affiliations

[1]Department of Pathology, School of Clinical Medicine, the University of Hong Kong, Hong Kong.

[2]State Key Laboratory of Liver Research, The University of Hong Kong, Hong Kong.

[3]Centre for Oncology and Immunology, Hong Kong Science Park, Hong Kong.

[4]Department of Clinical Oncology, The University of Hong Kong-Shenzhen Hospital, Shenzhen, China

[5]Guangdong-Hong Kong Joint Laboratory for RNA Medicine, Sun Yat-Sen University, Guangzhou, China.

#Equal contribution

Corresponding author

Carmen Chak Lui Wong

Address: T810, 8/F, Block T, Queen Mary Hospital, Hong Kong

Phone number: +852-22552689

Email address: carmencl@pathology.hku.hk, cclwong@hku.hk

Conflict-of-interest statement

The authors have declared that no conflict of interest exists.

Abstract

Cell cycle inhibitors have a long history as cancer treatment. Here, we reported that these inhibitors combated cancer partially via Stimulator of IFN genes (STING) signaling pathway. We demonstrated that Paclitaxel (microtubule stabilizer), Palbociclib (cyclin dependent kinase 4/6 inhibitor), AZD1152 and GSK1070916 (aurora kinase B inhibitors) have anti-cancer functions beyond arresting cell cycle. They consistently caused cytosolic DNA accumulation and DNA damage, which inadvertently triggered the cytosolic DNA sensor DEAD-box helicase 41 (DDX41) and activated STING to secrete pro-inflammatory senescence-associated secretory phenotype factors (SASPs). Interestingly, we found that DDX41 was a transcriptional target of HIF. Hypoxia induced expression of DDX41 through HIF-1, making hypoxic HCC cells more sensitive to the anti-mitotic agents in STING activation and SASP production. The SASPs triggered immune cell infiltration in tumors for cancer clearance. The treatment of cell cycle inhibitors, especially Paclitaxel, extends survival by perturbing mouse HCC growth when used in combination with anti-PD-1. We observed a trend that Paclitaxel suppressed $STING^{WT}$ HCC more effectively than $STING^{KO}$ HCC, suggesting that STING might contribute to the anti-tumor effects of Paclitaxel. Our study revealed the immune-mediated tumor-suppressing properties of cell cycle inhibitors and suggested combined treatment with immunotherapy as a

potential therapeutic approach.

Introduction

Hepatocellular carcinoma (HCC) is the sixth most common cancer incidence and the third most common cause of cancer mortality worldwide (1). Cell cycle perturbation is often associated with carcinogenesis and malignant transformation and is a known feature of cancer (2, 3). Chemotherapy is one of the approaches which has been used to treat cancer for more than 50 years by inducing programmed cell death via cytotoxic or targeted manner (4). The classical cytotoxic therapies involve the use of Paclitaxel (Pac, microtubule stabilizer) and Palbociclib (Palbo, cyclin-dependent kinase (CDK) 4 and 6 inhibitor), which have been approved by FDA for treating ovarian carcinoma, breast carcinoma, non-small cell lung carcinoma (NSCLC) and AIDS-related Kaposi's sarcoma (5), and breast cancer respectively (6). Yet their effect towards HCC is still unclear as they are still on phase II clinical trials (NCT02423239 & NCT04175912) (NCT01356628). Other cell cycle inhibitors such as aurora kinase inhibitors (GSK1070916 (GSK) and AZD1152 (AZD)) are now undergoing clinical trials and being investigated as potential therapies (7). However, some studies revealed that HCC built resistance towards Paclitaxel (8, 9) and a phase II clinical study showed that Paclitaxel did not bring any survival advantage to HCC patients (10). Besides, two out of three clinical trials of AZD1152 on advanced solid tumor were terminated as the efficacy of AZD1152 monotherapy was not sufficient to support the continuity of

research (NCT00497679, NCT00338182 and NCT00497731), suggesting the cell cycle inhibitors in general might not be beneficial to HCC as monotherapy and other approaches for example combination therapy with other tyrosine-kinase inhibitors (TKIs) or immune checkpoint inhibitors (ICIs) might be needed for enhancing the effect of cell cycle inhibitors.

Since HCC is refractory to chemotherapies, systemic therapies are adopted for advanced HCC (11). The FDA approved first line therapies, including the TKIs Sorafenib and Lenvatinib, benefit the advanced HCC patients with extended overall survival (OS) of three months only, while the second line therapies increase OS of 1.6 – 2.8 months in tumor-progressing Sorafenib-treated patients (12, 13).

The emergence of ICIs in the past few years showed better efficacy over the traditional TKI regimen and the FDA has recently approved a combination of ICI Atezolizumab and anti-VEGF antibody Bevacizumab as first-line therapy with better median OS compared to Sorafenib (13-15). However, the results of other ICIs monotherapy for instance anti-programmed cell death 1 (PD-1), were not so promising and did not improve the survival endpoint due to low response rate (12, 16). Hence in this study, we aimed to figure out new combination therapies to boost the efficacy of current

medication.

Stimulator of IFN genes protein (STING) is an adaptor protein involved in antiviral signaling pathway. It triggers the expression of type 1 IFN to initiate innate immune response (17-21). Our previous study showed that polo like kinase 4 (PLK4) inhibitor caused micronuclei-induced cytosolic DNA which triggered the expression of senescence-associated secretory phenotype factors (SASPs) via DEAD-box helicase 41 (DDX41) – STING – TANK-binding kinase 1 (TBK1) – Interferon regulatory factor 3/7 (IRF3/7) – NFκB pathway to activate immune response (22). Here we would like to explore if this mechanism can be generally applied to other well-known but mechanistically distinct inhibitors targeting different cell cycle phases, through apoptosis-mediated DNA release which would further activate DDX41-STING pathway. This response was even more dramatic under hypoxic condition which was usually found in solid tumors. Our study opened the avenue of combining cell cycle inhibitors with ICIs to halt the cell proliferation and concurrently unleash the full potential of immune cells to eradicate cancer.

Results

Over-expression of key cell cycle regulators in HCC is correlated to poor overall survival

The Cancer Genome Atlas (TCGA) data showed that the gene expression levels of *TUBB* (tubulin), *AURKB* (aurora kinase B), *CDK4* and *CDK6* are all up-regulated in HCC tissues as compared to corresponding non-tumor (NT) liver tissues (Fig 1A). The expression levels of these cell cycle proteins in HCC patients are negatively correlated to overall and disease free survival (Fig 1B). This showed the importance of cell cycle proteins in HCC development and patient overall survival by promoting cell growth and proliferation. Accordingly, impeding the cell cycle by targeting these proteins using inhibitors may block and cease HCC development.

Cell cycle inhibitors led to genome instability, DNA damage and cytosolic DNA accumulation in HCC cells

Cell cycle perturbation and genome instability

Cell cycle profiles were determined to monitor the effect of different cell cycle inhibitors. Paclitaxel, GSK1070916, AZD1152 and Palbociclib were used to interrupt the cell cycle progression of double thymidine synchronized-HCC cell lines MHCC97L cells and CLC4. Their cell cycle profiles were monitored by flow cytometry. The DNA

content of cell shifted from 2N to 4N after 12 hours in MHCC97L and 24 hours in CLC4. Furthermore, a broad peak ranging from 2N to 8N was observed 36 hours in MHCC97L, and 48 hours in CLC4 after treatment of Paclitaxel (Fig 1C, Supp fig 1). Similar results were obtained with AZD1152 and GSK1070916 where 8N and 16N peak appeared in both MHC97L and CLC4 after 48 hours and 72 hours respectively. Palbociclib showed a different profile where the peak shifted back to 2N after 24 hours and no 8N or 16N peak were observed. The presence of aneuploidy that indicated by broad peak ranging between 2N and 4N, and between 4N and 8N peak and the polyploidy that indicated by 8N and 16N peaks suggested most but not all anti-mitotic agents caused accumulation of genome instability in cells.

Increase of ROS level

The cytotoxic property of the cell cycle inhibitors might also boost their genotoxicity. The inhibitors might introduce oxidative stress to the cells by generating ROS (23-25). We examine whether the inhibitors bring oxidative stress to the cells by detecting the cellular ROS level using CM-H_2DCFDA, a fluorogenic dye that becomes highly fluorescent after being oxidized by ROS in cell. The cellular ROS level increased after treating the cells with the inhibitors, suggesting the inhibitors were cytotoxic and generated oxidative stress in the HCC cells (Supp fig 2).

DNA damage

The improper cell division and the accumulation of extensive DNA might introduce stress in chromosome and caused DNA damage and accumulation of DNA in cytoplasm. The build-up of cellular ROS could also cause harm to DNA by intensifying the replication stress, generating DNA double-strand breaks, hampering DNA repair, oxidizing the nucleoside bases and promoting oxidative DNA damage (26, 27). Therefore, we examined if DNA damage occurred in cells using gamma histone 2A.X (γ-H2A.X) as the DNA damage marker. Both immunofluorescent (IF) data (Fig 1D and supp fig 3) and western blot (Fig 1E) showed an increase in γ-H2A.X level, in cell cycle inhibitor treated cells, confirming the inhibitors induced DNA damage in cells.

Apoptosis

Genome integrity is indispensable for the proliferating of life. Chromosome mis-segregation induced aneuploidy and polyploidy, promoted chromosome instability and affected the maintenance of genome integrity and eventually led to programmed cell death – apoptosis (28). Besides, other cellular stress such as DNA damage, hypoxia and oxidative stress that brought by increased ROS would also provoke apoptosis. Hence, we detected the cell cycle inhibitor-induced apoptosis by using Annexin V and

propidium iodide (PI) assay, which discriminates live cells from early and late apoptotic cells. We found that all the inhibitors generated apoptotic cell death in MHCC97L cells (Supp fig 4). Z-VAD-Fmk (ZVF) is a pan-caspase inhibitor which inhibits apoptosis. The apoptosis could be rescued by ZVF, further confirming that the cell cycle inhibitors induced cell death through apoptosis.

Cytosolic DNA accumulation

We compared the relative amount of genomic DNA (gDNA) in cytoplasm to see if cell cycle inhibitors caused DNA accumulation in cytoplasm. The cytosolic gDNA isolated from the cells was measured using quantitative PCR (qPCR) and normalized to total gDNA. The qPCR data showed the gDNA content detected in cytoplasm increased significantly after drug treatment (Fig 1F). Our data demonstrated that only Paclitaxel and aurora kinase B inhibitors induced aneuploidy and polyploidy (Fig 1C), and all inhibitors caused accumulation of cytosolic gDNA.

Since apoptosis involves DNA fragmentation by caspase-activated DNase (CAD), the fragments may leak from the nucleus and contribute to accumulation of cytosolic DNA (29-32). In order to verify this hypothesis, we suppressed apoptosis by using the ZVF to see if the accumulation of gDNA in cytoplasm was abolished. We found that ZVF

substantially reduced the cytosolic gDNA level in the presence of cell cycle inhibitors confirming that apoptosis was essential for the build-up of cytosolic gDNA and indicating it was the major source of cytosolic gDNA (Fig 1F).

Cell cycle inhibitors induced cellular senescence and SASP secretion

Senescence occurs when cells enter permanent growth arrest and become non-proliferative. Since it can be induced by stress for example oxidative stress and DNA damage (33), we examine if cell cycle inhibitors induce cellular senescence by detecting senescence-associated β-galactosidase (SA-β-Gal) activity in cells which is indicated by blue color (Fig 2A). The cells turned blue after treatment with the cell cycle inhibitors and the morphology of cells became flat and enlarged showing that the cells underwent senescence in the presence of all inhibitors. Since senescent cells secrete SASPs, we detected the mRNA level of SASPs in cells under different inhibitors using RNA sequencing (Fig 2B). Only top 20 SASP genes with highest fold change in mRNA level were shown in the plot and the data illustrated all inhibitors promoted expression of different SASPs. Among the four inhibitors, the expression of c-c motif chemokine ligand 2 (CCL2) increased the most and thus in the later experiments, CCL2 was used as the representative of SASP. Gene set enrichment analysis (GSEA) also showed the expression of SASP gene set was upregulated under treatment of Paclitaxel, AZD1152

and Palbociclib. Since SASP consists of cytokines and chemokines which take part in inflammatory and immune response, we analyzed the gene set of inflammatory response, cytokine, TNFa signaling via NFκB and IL6-JAK-STAT3 signaling, and found that they were also enriched in presence of cell cycle inhibitors (Fig 2C and supp fig 5). In addition, these anti-mitotic agents also upregulated CCL2 mRNA level in CLC4 cells (Supp fig 6).

Cell cycle inhibitors induced SASP secretion via DDX41-STING pathway

It has been reported that the DNA sensor DDX41 was able to sense cytosolic DNA and activate STING-TBK1-IRF3/7 pathway to induce SASP expression (22). Upon activation by DDX41, STING dimerized in V-shape and translocated from ER to Golgi apparatus to recruit TBK1. TBK1 phosphorylated STING and further phosphorylated and recruited IRF3/7 and NFκB to nucleus for transcription of IFN-β, IL-6 and TNF (18-21). Hence, we determined whether this pathway was used in the case of cell cycle inhibitor treatment by knocking down (KD) the prime components in the pathway. Both qPCR and ELISA data illustrated that KD of *DDX41*, *STING1*, *IRF7* and *RelA* (transcription factor p65, subunit of NFκB) abrogated expression of CCL2 (Fig 3A, supp fig 7A and B). Flow cytometry data demonstrated the phosphorylation of STING and IRF3 after cell cycle inhibitor treatment in both MHCC97L and CLC4 (Fig 3B,

supp fig 8) and the western blot data showed that cell cycle inhibitors caused STING dimerization in time-dependent manner (Fig 3C). Our data suggested that cell cycle inhibitor caused accumulation of DNA in cytoplasm which triggered DDX41 to activate STING-TBK1-IRF3/7 pathway to initiate SASP secretion.

Hypoxia further exaggerated the effect of cell cycle inhibitors on SASP secretion

TCGA data revealed that up-regulation of *DDX41* is correlated with poor overall survival in HCC patients (Fig 4A). The high *DDX41* level is also associated with higher Buffa and Winter hypoxia score (Fig 4B), suggesting DDX41 may be hypoxia related. Hypoxia is defined as the reduction of oxygen availability or oxygen partial pressure that hampers the tissue or cell function, which can be caused by cancer (34). Thence we checked the *DDX41* mRNA level in different HCC cell lines under hypoxia to see if *DDX41* is induced. We found that *DDX41* was upregulated under hypoxia in most of the HCC cell lines but not MIHA, the immortalized human hepatocytes (Fig 4C). Since most of the hypoxic events are regulated by hypoxia-inducible transcription factor 1 (HIF-1), which mainly comprises of HIF-1α and HIF-1β, we verified if the hypoxic-induced expression of *DDX41* was regulated by HIF. Knockout (KO) of *HIF1A* and KD of *HIF1B* in MHCC97L cells suppressed the up-regulation of *DDX41* under hypoxia (Fig 4D). The expression of DDX41 was upregulated under hypoxia in NTC and

Knockdown (KD) group when compared to normoxic condition in CLC2. However, KD of *HIF1A* in CLC2 and CLC4 HCC cell lines also impaired the expression of *DDX41* in hypoxia compared to NTC control (Fig 4D). Then we ask if *DDX41* is a direct target of HIF. Five putative hypoxia-response elements (HREs) were found in the promoter region of *DDX41* and were designed to be covered by three primer pairs (Fig 4E). Chromatin immunoprecipitation (ChIP) assay revealed the enrichment of HIF-1α binding to HRE of *DDX41* only under hypoxia while the binding of HIF-1β to *DDX41* was enriched in both normoxic and hypoxic conditions (Fig 4F). Western blot confirmed the augmented DDX41 protein expression under hypoxia where the expression was reduced when *DDX41* was knocked down or when *HIF1A* was knocked out (Fig 4G). These results showing the expression of DDX41 was regulated directly under hypoxia via HIF-1α and HIF-1β. We asked whether cell cycle inhibitors could elicit the cytosolic DNA sensing to activate transcriptions of SASP in hypoxic HCC cells as DDX41 is directly regulated by HIF-1. The qPCR data evidenced that the expression of *CCL2* in cell cycle inhibitor treated cells was elevated significantly under hypoxia after Paclitaxel, AZD1152, GSK1070916 and Palbociclib treatments. The increment was repressed when *DDX41* was KD (Fig 4H). Our data demonstrated that the effect of cell cycle inhibitors on SASP expression was boosted significantly in hypoxic tumor due to the upsurge of HIF-regulated DDX41.

Cell cycle inhibitors induced immune surveillance in HCC tumors and promoted survival in combination with ICI

SASP consisting of chemokines, cytokines, proteases and growth factors are believed to be pro-inflammatory and initiate immune response (35-37). In order to verify if cell cycle inhibitors generally induced SASP expression triggered immune response, C57BL/6N immuno-competent mice were used for *in vivo* experiments. HCC was induced in mice using hydrodynamic tail vein injection (HDTVi) model with CRISPR-Cas9 system to KO transformation-related protein 53 (*Trp53*) and with Sleeping Beauty transposon system to over-express (OE) *c-Myc* ($Trp53^{KO}/c\text{-}Myc^{OE}$). The IF staining of glucose transporter 1 (Glut1), the hypoxia marker, in mice $Trp53^{KO}/c\text{-}Myc^{OE}$ tumor tissue verified the hypoxic environment in tumor (Supp fig 9A). AZD1152 and GSK1070916 are both ATP-competitive Aurora Kinase B inhibitor. Additionally, AZD1152 has been studied clinically, with 15 trials in phases I, II and III to date, in various cancer models (38). Therefore, we performed the drug treatment with AZD1152 for *in vivo* experiments. The mice were administrated with Paclitaxel, AZD1152 or Palbociclib three weeks after HDTVi. All the three cell cycle inhibitors significantly reduced the HCC tumor size without causing weight loss or adverse effect of mice (Fig 5A and supp fig 9B). H&E staining of HCC tissues in AZD1152 and Palbociclib

experiments showed that the tumor growth front of vehicle control treated groups (Ctrl) was generally more irregular when compared to the cell cycle inhibitor treated groups, while there was no difference between Ctrl and inhibitor treated groups in Paclitaxel experiment (Supp fig 10A and supp table 1-3). Further, venous invasion was only present in Ctrl groups in all three (Paclitaxel, AZD1152, Palbociclib) experiments (Supp fig 10B and supp table 1-3). The IHC staining of the mice HCC tumors clearly uncovered the profound increase of CD4 T cell, CD8 T cell and NK cell staining within tumor boundary (Fig 5B and supp fig 11). In addition, these cell cycle inhibitors upregulated a panel of senescence markers and SASPs in tumor core after treatment, as shown by the RNA sequencing data of mouse tumor tissues (Supp fig 12). In general, we observed a differential expression of the senescence signatures in different treatment groups. However, the trend of induction of SASP was consistently observed in mice after Paclitaxel/ Palbociclib/ AZD1152 treatments. These indicated the cell cycle inhibitors promoted the infiltration of both innate immune cells, i.e. NK cells, and adaptive immune cells, i.e. CD4 and CD8 T cells into tumor core. Their cytotoxic activities also contributed to cancer cell clearance and the consequential reduction of tumor sizes. The activation of immune surveillance in tumor provided it with a favorable condition to combine cell cycle inhibitor treatment with immunotherapy to fully unleash the potential of immune cells for cancer clearance. Therefore, an ICI, anti-

PD-1, was administrated in combination with the cell cycle inhibitors on C57BL/6N mice with HDTVi induced *Trp53*^{KO}/*c-Myc*^{OE} HCC. The survival results illustrated that minimal differences in term of overall survival between the untreated and single treatments were observed, however the combo treatment of Paclitaxel plus ICI arm notably extended overall survival of mice bearing HCC. AZD1152 and Palbociclib plus ICI arm tend to improve overall survival of the mice. (Fig 5C and supp fig 9C). This further confirmed the potential of combination treatment of cell cycle inhibitor with ICI in combating HCC. We observed that Paclitaxel extended the survival of mice with *Sting*^{WT} HCC and the trend was less clear in Sting^{KO} HCC (Fig 5D and supp fig 9D). It is worth noting that this set of data on the effects of Paclitaxel on *Sting*^{WT} HCC and *Sting*^{KO} HCC has not reached statistical significance. Therefore, it could not provide direct evidence that cell cycle inhibitors activate STING. However, the data implies that cell cycle inhibitors elicited anti-tumor effects partially through STING.

Discussion

Boosting the efficacy of current cell cycle inhibitors in HCC cancer treatment

Cell cycle inhibitors are potent chemotherapeutic drugs towards various cancer types except HCC. There are many cell cycle inhibitors available in the pharmaceutical market targeting different phases of cell cycle.

HCC may develop resistance to the inhibitors and some clinical trials implied that monotherapy did not work well on HCC (8-10) (NCT00497679, NCT00338182 and NCT00497731). Nonetheless, our paper demonstrated that all mechanistically distinct cell cycle inhibitors consistently have cell cycle independent potential to be used in combination with ICIs. Apart from the canonical intrinsic effect of cell cycle arrest, senescence and cell death, all the cell cycle inhibitors we tested simultaneously induce cytosolic DNA and trigger DDX41-STING pathway for secretion of pro-inflammatory SASP. The activation of STING pathway has been reported to promote the maturation, transition and activation of T cells, dendritic cells and NK cells (39). Our results demonstrated that cell cycle inhibitors recruited cytotoxic immune cells including CD4 T cells, CD8 T cells and NK cells to infiltrate into tumor core. Cytotoxic T lymphocytes (CTL) and NK cells are the principal players for cancer immunosurveillance and the subsequential eradication of cancer cells during immune response (40). They both attack tumor cells in a similar manner. During direct killing, CTLs use exocytosis to deliver granzymes and pore-producing perforin, and meanwhile secrete Fas-ligand and TRAIL to induce cell death of target cells. For indirect killing, they express pro-inflammatory cytokines and chemokines to recruit other immune cells for tumor clearance (41-44).

The ICIs anti-PD-L1 and anti-PD-1 are aimed to overcome the tolerance of T cells towards cancer clearance. Since NK cells possess PD-1, NK cells can also be activated by anti-PD-1 therapy (45). A study showed that anti-PD-L1 and anti-PD-1 activate exhausted NK and T cells by rerouting their metabolic pathways, thereby unleashing their cytotoxicity against tumor cells (42). Here we linked cell cycle perturbation with innate and adaptive immunity and enhanced the effect of cell cycle inhibitors by boosting the cytotoxicity of CTL and NK cells with ICIs.

Effect of hypoxia on cancer development

Oxygen consumption is crucial in tumor to provide satisfactory amount of energy by constant ATP production to support the rapid proliferation and thus tumor tends to grow near blood vessels. However, the tumor may propagate so fast that it outgrows the supply of blood and oxygen in chronic hypoxia (34). The oxygen level in liver appears in a gradual decrease from area around hepatic artery to that around portal vein and further to vein (46). The metabolic functions are impaired when the median oxygen partial pressure in tumor tissue drops (47). On one hand, hypoxia may retard growth and induce cell death by disrupting DNA repair and initiating cell cycle arrest, apoptosis or necrosis through increasing p53; while on the other hand, it may promote growth and survival by facilitating the adaptation of cells to stress through HIF e.g., inducing glycolysis, angiogenesis and anaerobic metabolism, and allowing tumor cell migration

and metastasis by aiding cell detachment, epithelial-mesenchymal transition and adhesion (34, 47, 48). Although hypoxia can promote inflammation and cause immune cells infiltration, it rather facilitates recruitment of immune cells with pro-tumor immune subsets over anti-tumorigenic ones, leading to tumor evasion from immunosurveillance and tumor aggression (49-51). Besides, hypoxia was suggested to be related to the resistance towards chemotherapy and radiotherapy and was responsible for the poor therapeutic outcome (34). As a result, hypoxia may be considered as a double-edge sword where it may induce cell death and suppress tumor growth, but on the contrary may promote angiogenesis and support tumor growth.

We are the first group to report *DDX41* as a HIF-regulated gene which is up-regulated under hypoxia. Since up-regulation of *DDX41* is associated with poor survival, and hypoxia is associated with chemotherapy and radiotherapy resistance and poor therapeutic outcome (34), both hypoxia and DDX41 are considered disadvantageous to HCC patients. Cell cycle inhibitors in this situation act as an imperative juncture to twist the harmful DDX41 and detrimental hypoxia into a constructive and valuable tool to combat cancer cells. Cell cycle inhibitors, by triggering DNA accumulation in cytoplasm, activate DDX41, the cytosolic DNA sensor, which activates STING pathway and the subsequent antitumoral immune response. This makes the hypoxic

tumor become more vulnerable to cell cycle inhibitor treatment, and thus gaining the confidence of using cell cycle inhibitors in HCC therapy.

Potential of combined treatment of cell cycle inhibitors with Atezolizumab and Bevacizumab

Combination of ICI Atezolizumab and anti-VEGF antibody Bevacizumab is now the most effective first-line therapy for HCC (13, 15). However, antiangiogenic therapies, i.e. anti-VEGF, restrict blood vessel development and would elicit intratumoral hypoxia, which favors tumor growth (52-54). Bevacizumab is expected to induce intratumoral hypoxia due to its anti-angiogenic function. Meanwhile, we showed that cell cycle inhibitors work best in hypoxic condition as DDX41 was induced by HIFs, leading to increased transcription of SASP. Therefore, it is possible in the future that cell cycle inhibitors could be used in combination with Atezolizumab and Bevacizumab to achieve the most effective anti-tumor response in HCC.

We found that the effects of cell cycle inhibitors are far more than their canonical intrinsic cell cycle effect, like genome instability, ROS production, DNA damage, cytosolic accumulation, senescence and apoptosis. They also contribute to a remarkable secondary effect by triggering SASP expression via DDX41-STING-TBK1-IRF3/7

pathway. This leads to recruitment of both innate and adaptive cytotoxic immune cells to tumor core for cancer surveillance and elimination. The combination treatments of cell cycle inhibitors with ICIs showed enhanced effect against HCC especially in adverse hypoxic environment.

Methods

Sex as a biological variant

Male mice were used in this study due to a higher incidence of liver cancers among males worldwide (1). Currently, there are no reports about differences between tumor incidence and pathologies related to the animal model regarding sex as variant involved in this study. Thus, sex was not considered as a biological variable.

The Cancer Genome Atlas (TCGA)

The RNA sequencing data of 50 pairs of human liver HCC tissue samples with their corresponding non tumor (NT) tissue samples was obtained from TCGA through the Broad GDAC Firehose (Broad Institute). The RSEM normalized count was used to show the expression levels of *TUBB*, *AURKB*, *CDK4*, *CDK6* and *DDX41* between HCC and NT.

The overall and disease free survival data of HCC patients were obtained from TCGA, PanCancer Atlas via cBioPortal and Z-score of 0 was used as threshold to define the high and normal expression level of target genes. The survival data was determined using Kaplan-Meier method and was analyzed using log-rank (Mantel-Cox) test.

Cell lines and culture

Human HCC cell lines including PLC/PRF/5, Hep3B and HepG2, human immortalized hepatocyte cell line, MIHA, and human embryonal kidney cell line 293FT were acquired from American Type Culture Collection (ATCC). Human HCC cell lines Huh7 was gifted by Prof H. Nakabayshi from the School of Medicine in Hokkaido University and MHCC97L was gifted by Dr. Z. Y. Tang from Fudan University of Shanghai. CLC2, CLC4 and CLC13 were Chinese liver cancer cell lines which were gifted by Dr. Lijian Hui (Chinese Academy of Sciences, Shanghai, China) (55). All cell lines were tested to be mycoplasma-free.

Huh7, PLC/PRF/5 and 293FT was grown in Dulbecco's Modified Eagle Medium-high glucose (DMEM-HG) medium (Gibco) with 1% penicillin-streptomycin (P/S, Gibco) and 10% fetal bovine serum (FBS, Gibco). MHCC97L, Hep3B, HepG2 and MIHA were grown in DMEM-HG medium with sodium pyruvate (Gibco), 1% P/S and 10%

FBS. CLC2, CLC4 and CLC13 were grown in Roswell Park Memorial Institute (RPMI) 1640 medium (Gibco) with 1% P/S, 10% FBS, 1x Insulin-Transferrin-Selenium-Sodium Pyruvate (ITS-A) and 40 μg/L recombinant human epidermal growth factor (hEGF, PeproTech). All cell lines were incubated in 5% CO_2 at 37°C humidified incubator.

Stable cell line establishment

Human *DDX41*, *STING1*, *IRF7*, *RelA*, *HIF1A* and *HIF1B* KD in cells were produced using shRNAs mediated by lentivirus. The oligonucleotides (Integrated DNA Technologies, IDT) containing specific shRNA targets or non-target control (NTC) were put into pLKO.1-puro vector (Sigma), which were then transfected into the cells and followed by puromycin selection to generate stable KD cell lines. The KD efficiency of shRNA was validated by its mRNA expression using qPCR.

Human *HIF1A* KO cells were produced using TALEN. The specific TALE domain was put into pTALEN v2 vector, which was then transfected into the cells and followed by clonal expansion to generate stable KO cell lines. DNA sequencing and SURVEYOR mutation detection kit (Transgenomic, Inc.) were used to validate the TALEN-induced frame-shift mutation.

RNA extraction

$1e^6$ Cells were washed with PBS and incubated in 1 ml TRIzol reagent (Ambion® by Life Technologies) at room temperature for 5 min. For RNA extraction from mice tissues, frozen samples were homogenated in 1ml TRIzol reagent. After adding 200 µl chloroform, the sample was shaken vigorously for 15s and incubated at room temperature for 3 min. The sample was centrifuged for 15 min at 4 °C at 12,000 rpm. Around 500 µl upper layer was withdrawn and mixed with 500 µl isopropanol by vortexing. After 10 min incubation at room temperature, the sample was centrifuged for 10 min at 4 °C at 12,000 rpm. Supernatant was discarded and RNA pellet was washed with 1 ml 75% ethanol followed by 9,000 rpm centrifugation for 5 min at 4 °C twice. The pellet was left air-dry and then dissolved in 40 µl ultrapure distilled water with 55 °C incubation for 10 min. BioDrop™ µLITE spectrophotometer (BioDrop Ltd) was used to measure the RNA concentration. RNA samples were stored at -80 °C.

RNA sequencing

The RNA extracted were sent for paired-end Illumina HiSeq2000 sequencing (Axeq Technologies). For each sample, more than 1e5 cells were sequenced, respectively. TruSeq Stranded mRNA Sample Prep Kit (Illumina) was utilized to prepare the mRNA

library with poly(A)+. TopHat-Cufflinks pipeline was employed to handle the sequencing data and to express it in FPKM (fragments per kilobase of transcript sequence per million mapped reads), which was then analyzed using GSEA.

Reverse transcription and quantitative PCR (RT-qPCR)

1 μg RNA was utilized for reverse transcription using GeneAmp® PCR Reagent Kit (Applied Biosystems) according to the instruction from manufacturer and was converted to cDNA. The cDNA samples were stored at -20 ºC.

1 μl of the 10-fold diluted cDNA was used for qPCR and mixed with 5 μl SYBR Green qPCR Master Mix (Applied Biosystems), 0.2 μl 10 μM primer mix and 3.8 μl ultrapure distilled water. Human 18S was used as housekeeping gene. The qPCR reaction was run under StepOnePlus Real-Time PCR system (Applied Biosystems) at 95 °C for 15s, and 40 cycles of 60 °C for 1 min and 68 °C for 1 min.

Cytosolic gDNA analysis

Cells were collected and divided into two aliquots with equal cell number. For total DNA extraction, the cells were lysed in lysis buffer (25 mM EDTA, 10 mM Tris-HCl (pH 8.0), 0.5% SDS, 100 mM NaCl) and were ready for DNA extraction. For cytosolic

DNA extraction, cells were lysed for 10 min in permeabilization buffer (50 μg/mL digitonin (Thermo Fisher Scientific), 150 mM NaCl, 2 mM EDTA, 50 mM HEPES (pH 7.4)) and then centrifuged for 3 min at 1000 g. The supernatant was transferred to a new tube and centrifuged for 10 min at 17000 g. The supernatant was collected and was ready for DNA extraction. For DNA extraction of both total and cytosolic DNA, Phenol:Chloroform:Isoamyl alcohol (25:24:1, v/v, Invitrogen) was used. The extracted DNA was precipitated overnight at -20 °C by mixing with 7.5 M ammonium acetate, 100% ethanol and glycogen. The DNA was washed with 70% ethanol and the DNA pellet was left air-dry and then dissolved in ultrapure distilled water. Both cytosolic and total gDNA were quantified using qPCR with human 18S primers.

Chromatin immunoprecipitation (ChIP)

The cells were fixed in 1% (v/v) formaldehyde for 10 min at 37 °C. A final concentration of 125 mM glycine was added to sample and incubated for 5 min at 37 °C. After washing with PBS, the cells were lysed in ChIP lysis buffer and subjected to sonication. The sonicated DNA fragments were first incubated overnight at 4 °C with HIF-1α or HIF-1β antibodies, or IgG control, and then incubated with Protein A/ Salmon Sperm DNA Agarose Beads (Thermo Fisher Scientific). Buffer with different salt gradients were used to wash the beads. 1% SDS/$NaHCO_3$ was then used to elute

the DNA from beads which was then extracted using phenol-chloroform. The ChIP DNA was analyzed using qRT-PCR with primers flanking the HRE regions.

Protein extraction and western blotting (WB)

For whole cell protein extraction, the cells were washed with cold PBS and then collected in fresh cold PBS using cell scraper. The cells were centrifuged for 2 min at 4 °C 4000 rpm. The cell pellet was resuspended with radioimmunoprecipitation assay (RIPA) buffer (50 mM Tris-HCl (pH 7.4), 1 mM EDTA, 150 mM NaCl, 0.05% (w/v) SDS, 0.7% (v/v) NP-40). For detection of STING dimer, the cells NETN lysis buffer (20 mM Tris-HCl (pH 8), 0.5 mM EDTA, 100 mM NaCl, 0.5% (v/v) NP-40) was used. The cells were then incubated on ice together with the cocktails of cOmplete protease inhibitor (Roche) and PhosSTOP phosphatase inhibitor (Roche) for 15 min. The sample was centrifugated for 15 min at 4 °C 12000 rpm and the whole cell protein lysate in the supernatant was collected. Bradford protein assay (Bio-Rad Laboratories) was used to measure the protein concentration and bovine serum albumin (BSA) was used to generate the standard curve. The absorbance was measured at 595 nm using microplate reader. 40 μg protein lysate was used to prepare sample lysate by mixing with 6X SDS sample loading buffer and then boiled at 95 °C for 10 min. For detection of STING dimer, the lysate was mixed with sample loading buffer without β-mercaptoethanol.

For histone extraction, the cells were washed with cold PBS and then collected in triton extraction buffer (TEB) (0.02% (w/v) NaN_3, 2mM phenylmethylsulfonyl fluoride (PMSF), PBS containing 0.5% Triton X-100 (v/v)) using cell scraper. The cells were mixed gently and incubated on ice for 10 min. The sample was centrifugated for 10 min at 4 °C 500 g and the supernatant was discarded. The sample was washed with TEB twice and centrifugated for 10 min at 4 °C 500 g. The pellet was resuspended in 0.2 N HCl and incubated overnight at 4 °C with rotation for histone extraction. After centrifugation for 10 min at 4 °C 2500 g, the histone protein lysate in the supernatant was collected to measure the protein concentration using Bradford protein assay. 40 µg histone lysate was used to prepare sample lysate by mixing with 6X SDS sample loading buffer. The sample lysate was neutralized with NaOH and then boiled at 95 °C for 10 min.

Sodium dodecyl sulphate - polyacrylamide gel electrophoresis (SDS-PAGE, Bio-Rad Laboratories) was used to separate different proteins in the sample lysate. 10% acrylamide gel was used for whole protein lysate and 12% acrylamide gel was used for histone lysate. The gel was prepared using TGX FastCast premixed acrylamide solutions (Bio-Rad), N’, N’, N', N'-tetramethylethane-1,2-diamine (TEMED) and 10%

ammonium persulfate (APS) according to the manufacturer's protocol. After gel electrophoresis separation, the proteins were transferred to polyvinylidene difluoride (PVDF) membrane (GE Healthcare) by semi-dry Trans-Blot Turbo Transfer System (Bio-Rad) for 8 min at 25 V. The membrane was shaken in 5% non-fat milk with tris-buffered saline (TBS) and 0.1% (v/v) Tween 20 (TBST) for 1 h at room temperature. Specific primary antibody was prepared in 5% non-fat milk and was shaken with the membrane for overnight at 4 °C. The membrane was washed with shaking in 1x TBST at room temperature for 5 min 3 times and was then shook with specific horseradish peroxidase (HRP) conjugated secondary antibody for 2 h at room temperature. The membrane was washed with shaking in 1x TBST at room temperature for 5 min 3 times and then soaked in Amersham ECL Prime Western Blotting Detection Reagent (GE Healthcare) for 1 min at room temperature to generate chemiluminescent signals. The signal was then captured for analysis using Alliance Q9 Advanced chemiluminescence and spectral fluorescence imaging system (Uvitec).

Immunofluorescent (IF) imaging

Cells that seeded on cover slips in 6-well culture plate were washed with PBS and fixed in 4% (v/v) formaldehyde for 10 min at room temperature and then washed with shaking for 5 min 3 times with PBS. The cells were soaked in 0.5% Triton X-100 for

10 min at room temperature and then washed with shaking for 5 min 3 times with PBS. The cells were shaken in 3% BSA for 2 h at room temperature and stained with specific primary antibody overnight at 4 °C, followed by washing with shaking for 5 min 3 times with PBS. The cells were stained with specific secondary antibody for 2 h at 4 °C in dark and washed with shaking for 5 min 3 times with PBS. The cells on cover slips were mounted with glass slides in Prolong Diamond Antifade mountant with DAPI (Invitrogen). The slides were dried at 4 °C in dark overnight and then sealed with nail polish. The signal was then captured for analysis using Carl Zeiss LSM710 and LSM 880 confocal microscope (Zeiss). For analysis in each experimental condition, more than 85 cells were analysed for each experimental condition for micronuclei measurement. Two separate fields were quantified for each sample using ImageJ. The values of γ-H2A.X foci per nucleus were calculated by dividing the total number of γ-H2AX foci by the number of cell nuclei. The average values of the number foci per nucleus for each treatment group were normalized to control group.

Immunohistochemistry (IHC)

The mouse liver cancer tissue was fixed in 4% (v/v) formaldehyde overnight and then washed and kept in 70% ethanol before embedded in paraffin for slicing. The paraffin-embedded slices were dewaxed in xylene and then rinsed with 100%, 95% and 80%

ethanol. The slices were boiled for 15 min in 1 mM EDTA (pH7.8) to retrieve the antigen. 1x TBS was used to rinse the slices and the reaction was quenched by incubating the slices with 3% (v/v) H_2O_2 in 1x TBS for 30 min at room temperature. The slices were rinsed with 1x TBS and then incubated with 2x casein (Vector Laboratories) for 10 min at room temperature and after that stained with specific primary antibody overnight at 4 °C. The slices were washed with shaking in 1x TBST at room temperature for 5 min 4 times and was then stained with specific HRP conjugated secondary antibody (Agilent Technologies) for 30 min at room temperature. The slices were washed with shaking in 1x TBST at room temperature for 5 min 4 times and then immersed in 3', 3'-diaminobenzidine (DAB, Sigma-Aldrich) and H_2O_2 containing TBS. Once the signal developed, the slices were quenched with water. The slices were counterstained with haematoxylin, soaked in Scott's tap water and dehydrated in 80%, 95%, 100% ethanol and xylene sequentially. For histological study, hematoxylin and eosin staining were used. Section were finally mounted with cover slips for analysis.

Flow cytometry (FC)

Cells were collected in cell staining buffer (1x PBS, 2mM EDTA, 0.5% bovine serum albumin), then fixed and permeabilized in fixation buffer (BioLegend) and

permeabilization wash buffer (BioLegend) respectively. The cells were incubated with phospho-STING and phospho-IRF3 antibodies and the fluorophore signals were detected by BD LSR Fortessa Analyzer (BD Biosciences) and analyzed using computer software FlowJo.

Cell cycle profile

The cells were synchronized using double thymidine by treating with 2 mM thymidine (Calbiochem) in FBS-free culture medium for 18 h followed by releasing in full culture medium for 8 h and then treating with 2 mM thymidine in FBS-free culture medium for 16 h. MHCC97L were released in full culture medium with or without drug treatment for 12, 24, 36, 48 and 60 h. For CLC4, cells were treated with cell cycle inhibitors for 24, 48 and 72 h. Medium and drugs were replenished every alternative day. The cells were collected and fixed with 70% (v/v) ethanol at 4 °C overnight. The cells were then stained with 50 μg/ml propidium iodide (PI) (Sigma) and 20 μg/mL RNase A (Invitrogen) at 37 °C for 10 minutes in dark. The fluorophore signals were detected by BD LSR Fortessa Analyzer (BD Biosciences) and analyzed using computer software FlowJo.

Apoptosis assay

The cells together with the cell culture supernatant were collected and washed with PBS. Annexin V-FITC Kit (MBL International) was used to stain the cells according to manufacturer's instructions. In brief, the cells were stained with Annexin V binding buffer, Annexin V-FITC and PI for 15 min at room temperature in dark. The fluorophore signals were detected by BD LSR Fortessa Analyzer (BD Biosciences) and analyzed using computer software FlowJo.

ROS quantification

The cells were collected and washed with cold PBS and centrifuged for 1 min at 4 °C at 3,000 rpm. The cells were stained on ice with 2 μM chloromethyl-20,70-dichlorodihydrofluorescein diacetate (CM-H_2DCFDA, Life Technologies) in dark. The fluorophore signals were detected by BD LSR Fortessa Analyzer (BD Biosciences) and analyzed using computer software FlowJo.

Enzyme-linked immunosorbent assay (ELISA)

Human CCL2/MCP-1 Quantikine ELISA Kit (R&D systems) was used to quantify the amount of CCL2 secreted by cells in medium according to the manufacturer's protocol. In brief, the cell culture supernatant was collected and filtered with 0.45 μm filter to remove cell debris. The filtered supernatant was added to 96-well ELISA plate and

incubated for 2 h at room temperature. Each well was washed with wash buffer 3 times and incubated with human MCP-1 conjugate for 1 h at room temperature and then washed 3 times again. Substrate solution was added and incubated for 30 min in dark at room temperature, and followed by the addition of stop solution. The optical density was measured at 450 nm using microplate reader with wavelength correction at 570 nm. Four parameter logistic (4-PL) curve-fit was used to generate the standard curve for data analysis.

Senescence associated β-galactosidase (SA-β-Gal) activity assay

Senescence β-galactosidase staining kit (Cell Signaling Technology) was used to detect the activity of β-galactosidase in senescent cells according to the manufacturer's protocol. In brief, the cells were washed with PBS and fixed with fixative solution for 15 min at room temperature. The cells were then washed with PBS and stained with β-galactosidase staining solution at pH 6 for overnight at 37 °C in dry incubator in dark. The cell images were captured and analyzed using inverted microscope.

Hydrodynamic tail vein injection (HDTVi)

Male C57BL/6N mice with age of 8 to 10 week provided by the Centre for Comparative Medicine Research (CCMR) in the University of Hong Kong were used for HDTVi. A

mixture of plasmid DNA containing *Trp53* KO plasmid, *c-Myc* OE plasmid and sleeping beauty transposon plasmid were prepared in saline ($Trp53^{KO}$/$c\text{-}Myc^{OE}$). For *Sting* knock-out HCC model, *Trp53-Sting* KO plasmid was used instead of *Trp53* KO plasmid. The plasmid mixture of volume equaling to 10% mice body weight was injected within 7s into the lateral tail vein of mice. The drug treatment was started two to three weeks after HDTVi and the mice were weighted two to three times a week. At the experiment end point, the liver tumors were harvested and weighted. Male mice are used in this study due to a higher incidence of liver cancers among males worldwide (1). Currently, there are no reports regarding differences between tumor incidence and pathologies related to the animal model involved in this study.

Drug treatment

For in vitro assay, 10 nM Paclitaxel (P-9600, LC Laboratories), 50 nM GSK1070916 (HY-70044, MedChemExpress), 500 nM AZD1152-HQPA (SML0268, Sigma), 10 μM Palbociclib (P-7788, LC Laboratories) and 50 μM Z-VAD-FMK (S7023, Selleckchem) were used unless otherwise specified. All the drugs were reconstituted in DMSO.

For in vivo drug administration, Paclitaxel in DMSO was diluted in 60% PEG (Sigma) and was administered via intraperitoneal (IP) injection twice a week at 10 mg/kg.

AZD1152-HQPA in DMSO was diluted in 40% PEG and was administered via IP injection every 3 days at 10 mg/kg. Palbociclib was dissolved in ultrapure water and was administered orally daily at 75 mg/kg. Anti-PD-1 antibody (BE0146, BP0146, BioXCell) was diluted in saline and was administered via IP injection twice a week for 3 weeks at 10 mg/kg unless otherwise specified.

Statistics

All statistical analysis was determined using GraphPad Prism 8.0 software (GraphPad Software Inc.). The data was demonstrated as mean ± standard deviation and two-tailed Student's t-test, Wilcoxon signed-rank test, Kaplan–Meier test, Log rank (Mantel Cox) test, one-way and two-way ANOVA with Bonferroni correction were used for analysis when appropriated. Statistically significant P-value was defined at < 0.05, where * $p < 0.05$; ** $p < 0.01$; *** $p < 0.001$, **** $p < 0.0001$.

Study approval

All animal experimental procedures were reviewed and approved by the CCMR which is an AAALAC International accredited service centre of the Faculty of Medicine in the University of Hong Kong (CULATR protocol 4889-18).

Data availability

Patient data from online TCGA database was retrieved from http://www.cbioportal.org/. Next generation sequencing data are available in NCBI public repositories, the Sequence Read Archive (SRA) system (PRJNA1153299, PRJNA1153321). Supporting analytic code and all data points are available from the corresponding author upon request.

Author contributions

The conception and design of the study were contributed by Po Yee Wong, Cerise Yuen Ki Chan, Helen Do Gai Xue, and Carmen Chak Lui Wong. Acquisition, analysis and interpretation of data were performed by Po Yee Wong, Cerise Yuen Ki Chan, Helen Do Gai Xue, Chi Ching Goh, Jacinth Wing Sum Cheu, Aki Pui Wah Tse, Misty Shuo Zhang and Yan Zhang. Drafting of the manuscript was done by Po Yee Wong, Cerise Yuen Ki Chan, Helen Do Gai Xue, and Carmen Chak Lui Wong. Final approval of the version submitted for publication was decided by Carmen Chak Lui Wong.

Acknowledgments

We thank the CCMR of the University of Hong Kong in support of our animal experiments. We also thank the Imaging and Flow Cytometry Core of the Centre for

PanorOmic Sciences (CPOS) of the Li Ka Shing Faculty of Medicine, the University of Hong Kong for the technical support.

Funding

This work was supported by the National Natural Science Foundation of China - the Excellent Young Scientist Fund (Hong Kong and Macau) (82022077), Health and Medical Research Fund (08192516), Research Grant Council Collaborative Research Fund (RGC CRF) (C7008-22G) (C5106-23G), Research Grant Council Research Impact Fund (RGC RIF) (R5008-22), Research Grant Council Theme Based Research Scheme (RGC TBRS) (T12-716/22-R), Shenzhen Science and Technology Program (ZDSYS20210623091811035, KQTD20180411185028798), Sanming Project of Medicine in Shenzhen (SZSM202211017), Shenzhen Key Medical Discipline Construction Fund (SZXK014), the Centre for Oncology and Immunology under the Health@InnoHK initiative funded by the Innovation and Technology Commission, the Government of Hong Kong SAR, China. C.C.L.W is the recipient of the University of Hong Kong Outstanding Research Supervisor Award.

References

1. Internaltional Agency for Research on Cancer. Liver. https://gco.iarc.fr/today/data/factsheets/cancers/11-Liver-fact-sheet.pdf. Updated December, 2022. Accessed September 2, 2024.
2. Malumbres M, and Barbacid M. Cell cycle, CDKs and cancer: a changing paradigm. *Nat Rev Cancer.* 2009;9(3):153-66.
3. Suski JM, et al. Targeting cell-cycle machinery in cancer. *Cancer Cell.* 2021;39(6):759-78.
4. Sarosiek KA, et al. Mitochondria: gatekeepers of response to chemotherapy. *Trends Cell Biol.* 2013;23(12):612-9.
5. U.S. National Library Of Medicine. Paclitaxel - paclitaxel injection https://dailymed.nlm.nih.gov/dailymed/drugInfo.cfm?setid=9ffd3e34-537f-4f65-b00e-57c25bab3b01&audience=consumer. Updated October, 2022. Accessed September 2, 2024.
6. Food and Drug Aministration. Highlights of prescribing information. Ibrance (palbociclib) capsules, for oral use. https://www.accessdata.fda.gov/drugsatfda_docs/label/2017/207103s004lbl.pdf. Updated March 31, 2017. Accessed on September 2, 2024.
7. Petroni G, et al. Immunomodulation by anticancer cell cycle inhibitors. *Nat Rev*

Immunol. 2020;20(11):669-79.

8. Chae S, et al. Resistance to paclitaxel in hepatoma cells is related to static JNK activation and prohibition into entry of mitosis. *Am J Physiol Gastrointest Liver Physiol.* 2012;302(9):G1016-24.

9. Meena AS, et al. Inherent and acquired resistance to paclitaxel in hepatocellular carcinoma: molecular events involved. *PLoS One.* 2013;8(4):e61524.

10. Chao Y, et al. Phase II and pharmacokinetic study of paclitaxel therapy for unresectable hepatocellular carcinoma patients. *Br J Cancer.* 1998;78(1):34-9.

11. Villanueva A. Hepatocellular Carcinoma. *N Engl J Med.* 2019;380(15):1450-62.

12. Sperandio RC, et al. Hepatocellular Carcinoma Immunotherapy. *Annu Rev Med.* 2022;73:267-78.

13. Llovet JM, et al. Immunotherapies for hepatocellular carcinoma. *Nat Rev Clin Oncol.* 2022;19(3):151-72.

14. Food and Drug Aministration. FDA approves atezolizumab plus bevacizumab for unresectable hepatocellular carcinoma. https://www.fda.gov/drugs/resources-information-approved-drugs/fda-approves-atezolizumab-plus-bevacizumab-unresectable-hepatocellular-carcinoma Updated Jun 1, 2020. Accessed September 2, 2024.

15. Llovet JM, et al. Molecular therapies and precision medicine for hepatocellular

carcinoma. *Nature reviews Clinical oncology.* 2018;15(10):599-616.

16. Targeted Therapies in Oncology. ODAC Opposes Ongoing FDA Approval of Nivolumab for HCC in Patients Pretreated With Sorafenib. https://www.targetedonc.com/view/odac-opposes-ongoing-fda-approval-of-nivolumab-for-hcc-in-patients-pretreated-with-sorafenib Updated April 29, 2021. Accessed by September 2, 2024.

17. Briard B, et al. DNA Sensing in the Innate Immune Response. *Physiology (Bethesda).* 2020;35(2):112-24.

18. Christensen MH, and Paludan SR. Viral evasion of DNA-stimulated innate immune responses. *Cell Mol Immunol.* 2017;14(1):4-13.

19. Parvatiyar K, et al. The helicase DDX41 recognizes the bacterial secondary messengers cyclic di-GMP and cyclic di-AMP to activate a type I interferon immune response. *Nat Immunol.* 2012;13(12):1155-61.

20. Jiang Y, et al. The emerging roles of the DDX41 protein in immunity and diseases. *Protein Cell.* 2017;8(2):83-9.

21. Broz P, and Monack DM. Newly described pattern recognition receptors team up against intracellular pathogens. *Nat Rev Immunol.* 2013;13(8):551-65.

22. Chan CY, et al. Polo-like kinase 4 inhibitor CFI-400945 suppresses liver cancer through cell cycle perturbation and eliciting antitumor immunity. *Hepatology.*

2022.

23. Vijayaraghavan S, et al. CDK4/6 and autophagy inhibitors synergistically induce senescence in Rb positive cytoplasmic cyclin E negative cancers. *Nat Commun.* 2017;8:15916.

24. McCormick B, et al. MitoVitE, a mitochondria-targeted antioxidant, limits paclitaxel-induced oxidative stress and mitochondrial damage in vitro, and paclitaxel-induced mechanical hypersensitivity in a rat pain model. *Br J Anaesth.* 2016;117(5):659-66.

25. Jiang H, et al. Electrochemical Monitoring of Paclitaxel-Induced ROS Release from Mitochondria inside Single Cells. *Small.* 2019;15(48):e1901787.

26. Srinivas US, et al. ROS and the DNA damage response in cancer. *Redox Biol.* 2019;25:101084.

27. Ralph SJ, et al. The causes of cancer revisited: "mitochondrial malignancy" and ROS-induced oncogenic transformation - why mitochondria are targets for cancer therapy. *Mol Aspects Med.* 2010;31(2):145-70.

28. Borges HL, et al. DNA damage-induced cell death: lessons from the central nervous system. *Cell Res.* 2008;18(1):17-26.

29. Chang HY, and Yang X. Proteases for cell suicide: functions and regulation of caspases. *Microbiol Mol Biol Rev.* 2000;64(4):821-46.

30. Carneiro BA, and El-Deiry WS. Targeting apoptosis in cancer therapy. *Nat Rev Clin Oncol.* 2020;17(7):395-417.

31. Bacso Z, et al. The DNA of annexin V-binding apoptotic cells is highly fragmented. *Cancer Res.* 2000;60(16):4623-8.

32. Wang Y, et al. eccDNAs are apoptotic products with high innate immunostimulatory activity. *Nature.* 2021;599(7884):308-14.

33. Childs BG, et al. Senescent cells: an emerging target for diseases of ageing. *Nat Rev Drug Discov.* 2017;16(10):718-35.

34. Harris AL. Hypoxia--a key regulatory factor in tumour growth. *Nat Rev Cancer.* 2002;2(1):38-47.

35. Campisi J. Aging, cellular senescence, and cancer. *Annu Rev Physiol.* 2013;75:685-705.

36. Krizhanovsky V, et al. Senescence of activated stellate cells limits liver fibrosis. *Cell.* 2008;134(4):657-67.

37. Kang TW, et al. Senescence surveillance of pre-malignant hepatocytes limits liver cancer development. *Nature.* 2011;479(7374):547-51.

38. Antal H Kovacs, et al. Aurora B Inhibitors as Cancer Therapeutics. *Molecules* 2023; *28*(8), 3385

39. Li A, et al. Activating cGAS-STING pathway for the optimal effect of cancer immunotherapy. *J Hematol Oncol.* 2019;12(1):35.

40. Martinez-Lostao L, et al. How Do Cytotoxic Lymphocytes Kill Cancer Cells? *Clin Cancer Res.* 2015;21(22):5047-56.

41. Halle S, et al. Mechanisms and Dynamics of T Cell-Mediated Cytotoxicity In Vivo. *Trends Immunol.* 2017;38(6):432-43.

42. Wu SY, et al. Natural killer cells in cancer biology and therapy. *Mol Cancer.* 2020;19(1):120.

43. Shimasaki N, et al. NK cells for cancer immunotherapy. *Nat Rev Drug Discov.* 2020;19(3):200-18.

44. Oh DY, and Fong L. Cytotoxic CD4(+) T cells in cancer: Expanding the immune effector toolbox. *Immunity.* 2021;54(12):2701-11.

45. Myers JA, and Miller JS. Exploring the NK cell platform for cancer immunotherapy. *Nat Rev Clin Oncol.* 2021;18(2):85-100.

46. Wilson GK, et al. Hypoxia inducible factors in liver disease and hepatocellular carcinoma: current understanding and future directions. *J Hepatol.* 2014;61(6):1397-406.

47. Hockel M, and Vaupel P. Tumor hypoxia: definitions and current clinical, biologic, and molecular aspects. *J Natl Cancer Inst.* 2001;93(4):266-76.

48. Lu X, and Kang Y. Hypoxia and hypoxia-inducible factors: master regulators of metastasis. *Clin Cancer Res.* 2010;16(24):5928-35.

49. Eltzschig HK, and Carmeliet P. Hypoxia and inflammation. *N Engl J Med.* 2011;364(7):656-65.

50. Yuen VW, and Wong CC. Hypoxia-inducible factors and innate immunity in liver cancer. *J Clin Invest.* 2020;130(10):5052-62.

51. Riera-Domingo C, et al. Immunity, Hypoxia, and Metabolism-the Menage a Trois of Cancer: Implications for Immunotherapy. *Physiol Rev.* 2020;100(1):1-102.

52. Rapisarda A, et al. Increased antitumor activity of bevacizumab in combination with hypoxia inducible factor-1 inhibition. *Mol Cancer Ther.* 2009;8(7):1867-77.

53. Conley SJ, et al. Antiangiogenic agents increase breast cancer stem cells via the generation of tumor hypoxia. *Proc Natl Acad Sci U S A.* 2012;109(8):2784-9.

54. de Almeida PE, et al. Anti-VEGF Treatment Enhances CD8(+) T-cell Antitumor Activity by Amplifying Hypoxia. *Cancer Immunol Res.* 2020;8(6):806-18.

55. Qiu Z, et al. Hepatocellular carcinoma cell lines retain the genomic and transcriptomic landscapes of primary human cancers. *Sci Rep.* 2016;6:27411.

Figures

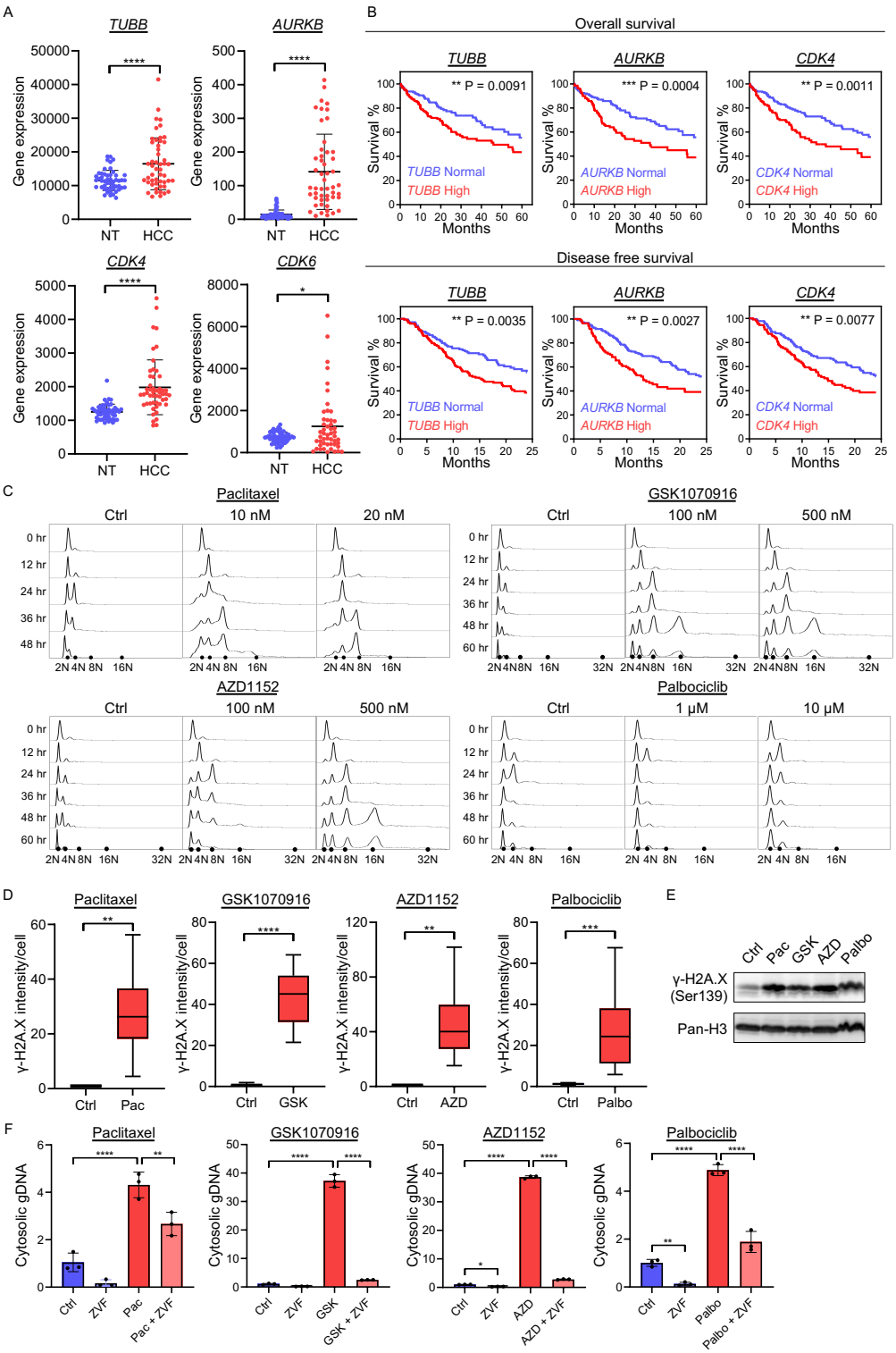

Figure 1. Cell cycle inhibitors led to genome instability, DNA damage and cytosolic

DNA accumulation in cell cycle regulators over-expressed HCC cells

A. TCGA data showing the up-regulated gene expression level (RSEM normalized count) of *TUBB* (tubulin), *AURKB* (aurora kinase B), *CDK4* and *CDK6* in HCC tissues compared to corresponding non-tumorous liver tissues (NT) in HCC patients (n=50/group). Scatter dot plot: mean with SD. Student's t test. **B.** TCGA data showing the correlation between HCC patients with normal or high expression level of *TUBB*, *AURKB* and *CDK4*, and the percentage of survival in overall survival and disease free survival model. The high expression level was defined as the target gene mRNA expression higher than the mean value ($Z > 0$). (n>300/plot). Log-rank (Mantel-Cox) test. **C.** The cell cycle progression of MHCC97L cells was synchronized at G1 phase using double thymidine synchronization method. After the cells released from second thymidine treatment at 0 hour time point, the cell cycle inhibitors with the indicated concentration were applied to the cells. The synchronized drug-treated cells were collected every 12 hours up to 60 hours. The DNA content was detected using propidium iodide (PI). Number of cells analyzed in each treatment (N) ≥ 10,000. **D - E.** MHCC97L cells were treated with cell cycle inhibitors for 48 hours. **D.** DNA damage was detected using γ-H2A.X in immunofluorescent (IF) staining. The signal intensity of γ-H2A.X per nucleus in inhibitors-treated cells was normalized to that in control (Ctrl) cells. Number of cells analyzed in each treatment (N) ≥ 85. Box and whiskers:

min to max. Student's t test. **E.** The cells were collected and histone was extracted. Western blot was used to show the protein expression level of γ-H2A.X and Pan-H3 was used as housekeeping protein. **F.** MHCC97L cells were treated with Paclitaxel, GSK1070916, AZD1152 or Palbociclib alone, ZVF alone or co-treated with both cell cycle inhibitors and ZVF for 72 hours. The cells were divided in two aliquots with equal cell number and were extracted for cytosolic DNA and total DNA. The gDNA in each portion was detected using qPCR with 18S primer. The cytosolic gDNA was determined by normalizing the relative expression of gDNA in cytoplasmic portion to that in total portion (n=3/group). Scatter dot plot: mean with SD. **A-D.** Student's t-test. F. One-way ANOVA with Bonferroni Correction. * $P < 0.05$, ** $P < 0.01$, *** $P < 0.001$, **** $P < 0.0001$.

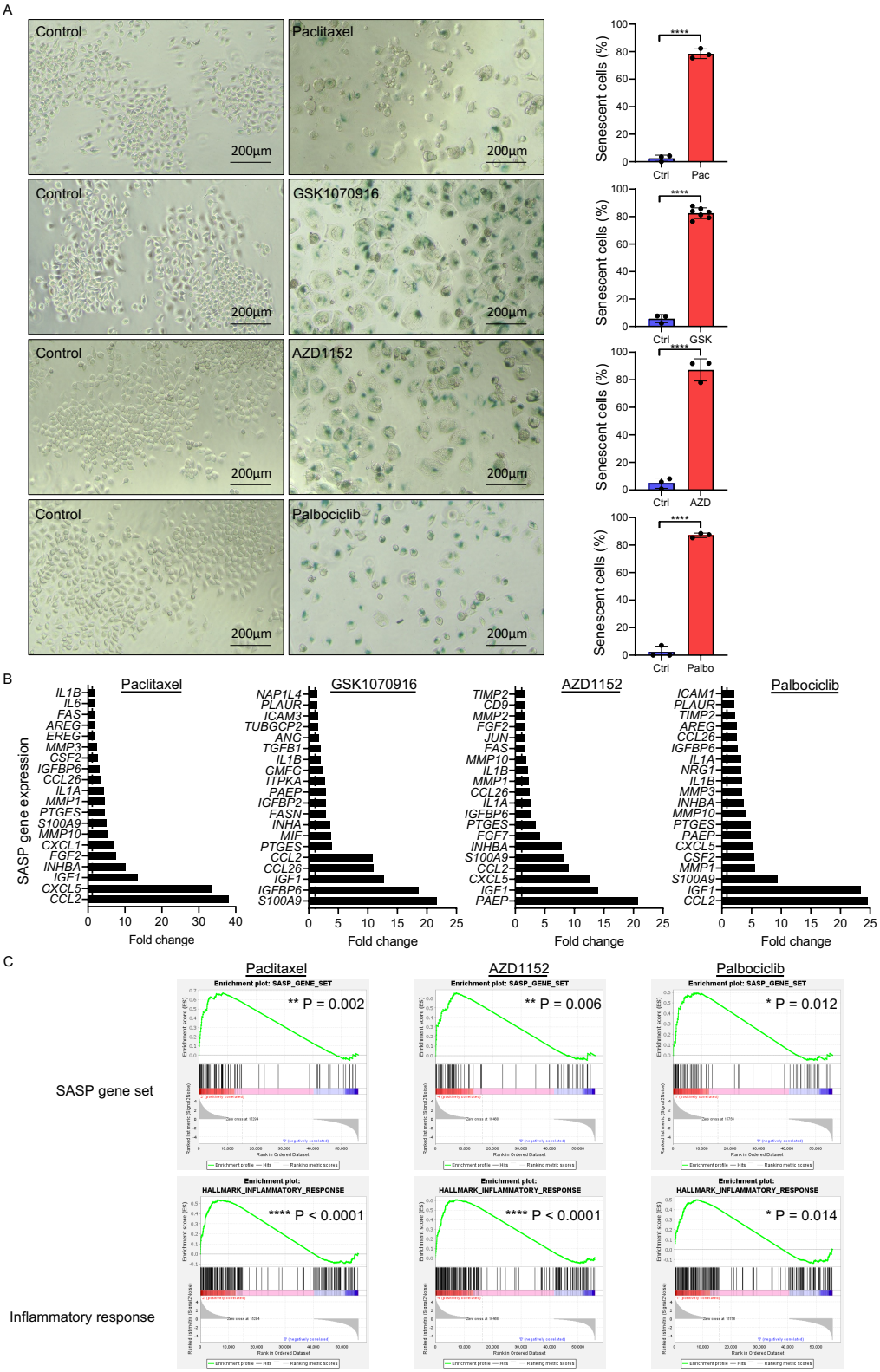

Figure 2. Cell cycle inhibitors induced cellular senescence and SASP secretion

MHCC97L cells were treated with cell cycle inhibitors for 96 hours. **A.** Senescent cells were detected using β-gal staining and cell images were captured and analyzed using inverted microscope. Transparent: non-senescence; Blue: senescence. Number of cells analyzed in each treatment (N) ≥ 200. Scale: 200 μm. Scatter dot plot: mean with SD. **B - C**. RNA was extracted and prepared for RNA sequencing. Number of cells analyzed in each treatment (N) ≥ 1e5. **B.** The fold change of the gene mRNA expression level was analyzed. The top 20 SASP genes with highest fold increase in expression level were extracted and visualized on graph. **C.** RNA sequencing data was used to analyze the enrichment of inflammatory response and SASP gene set using Gene Set Enrichment Analysis (GSEA). **A-C.** Student's t test. * $P < 0.05$, ** $P < 0.01$, *** $P < 0.001$, **** $P < 0.0001$.

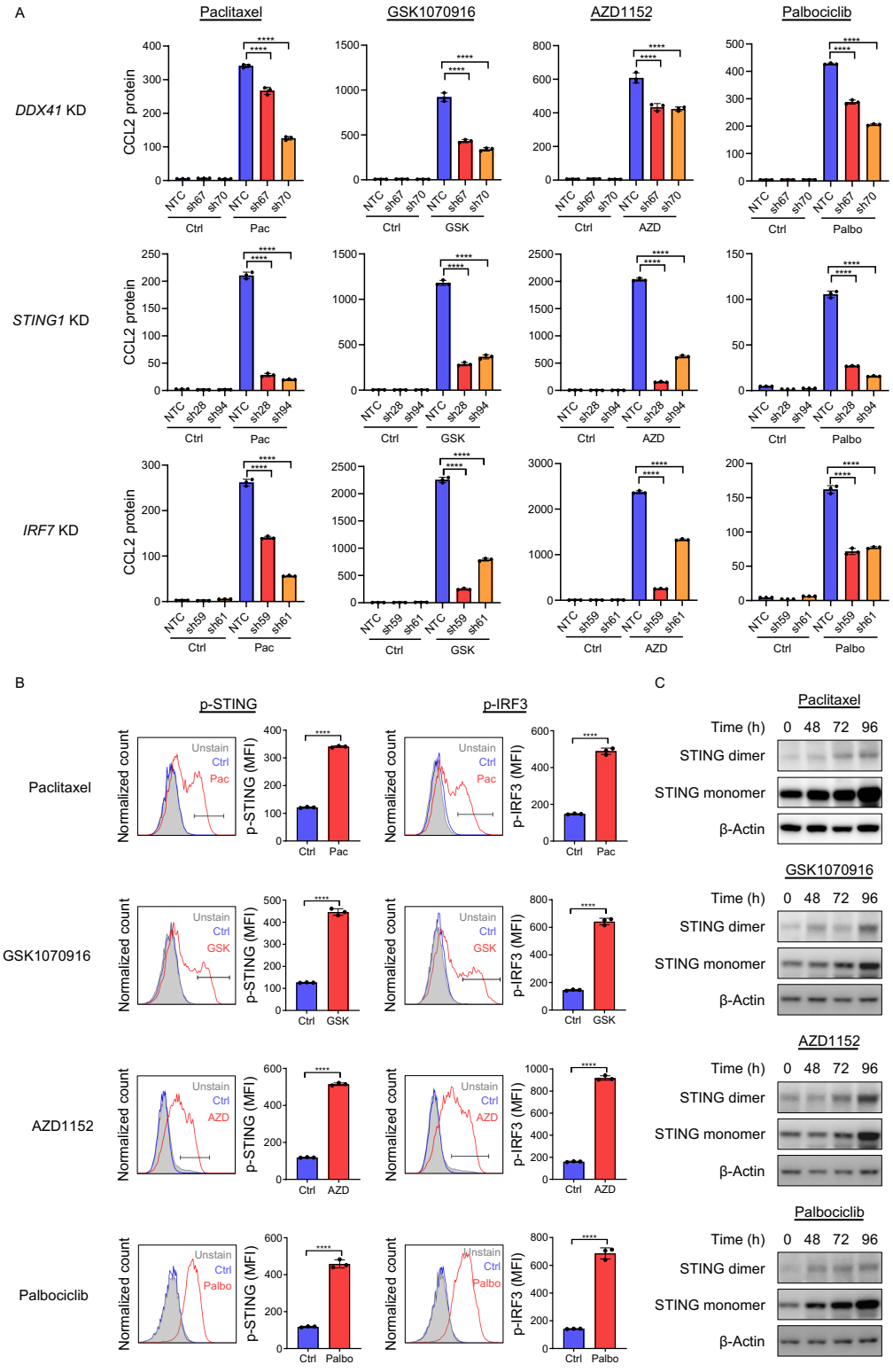

Figure 3. Cell cycle inhibitors induced SASP secretion via DDX41-STING pathway

A. MHCC97L stable KD clones of *DDX41*, *STING1* and *IRF7* KD were treated with cell cycle inhibitors for 96 hours and were released in drug-free medium with 2% FBS for 24 hours. The medium was collected and the cell numbers were counted. The concentration of CCL2 that secreted into the medium was determined using enzyme-linked immunosorbent assay (ELISA) assay. The CCL2 protein concentration was normalized to the cell number (pg / ml / 100,000 cell). **B.** MHCC97L cells were treated with 10 nM Paclitaxel, 100 nM GSK1070916, 100 nM AZD1152 or 10 μM Palbociclib for 96 hours. The phospho-STING (p-STING) and phospho-IRF3 (p-IRF3) were detected using specific antibodies and analyzed using flow cytometry (n=3/group). **C.** MHCC97L cells treated with cell cycle inhibitors were collected at indicated hours and the cell lysate was extracted. Western blot was used to show the protein expression level of STING monomer and dimer, and β-actin was used as housekeeping protein. Scatter dot plot: mean with SD. **A.** One-way ANOVA with Bonferroni Correction. **B.** Student's t test. * $P < 0.05$, ** $P < 0.01$, *** $P < 0.001$, **** $P < 0.0001$.

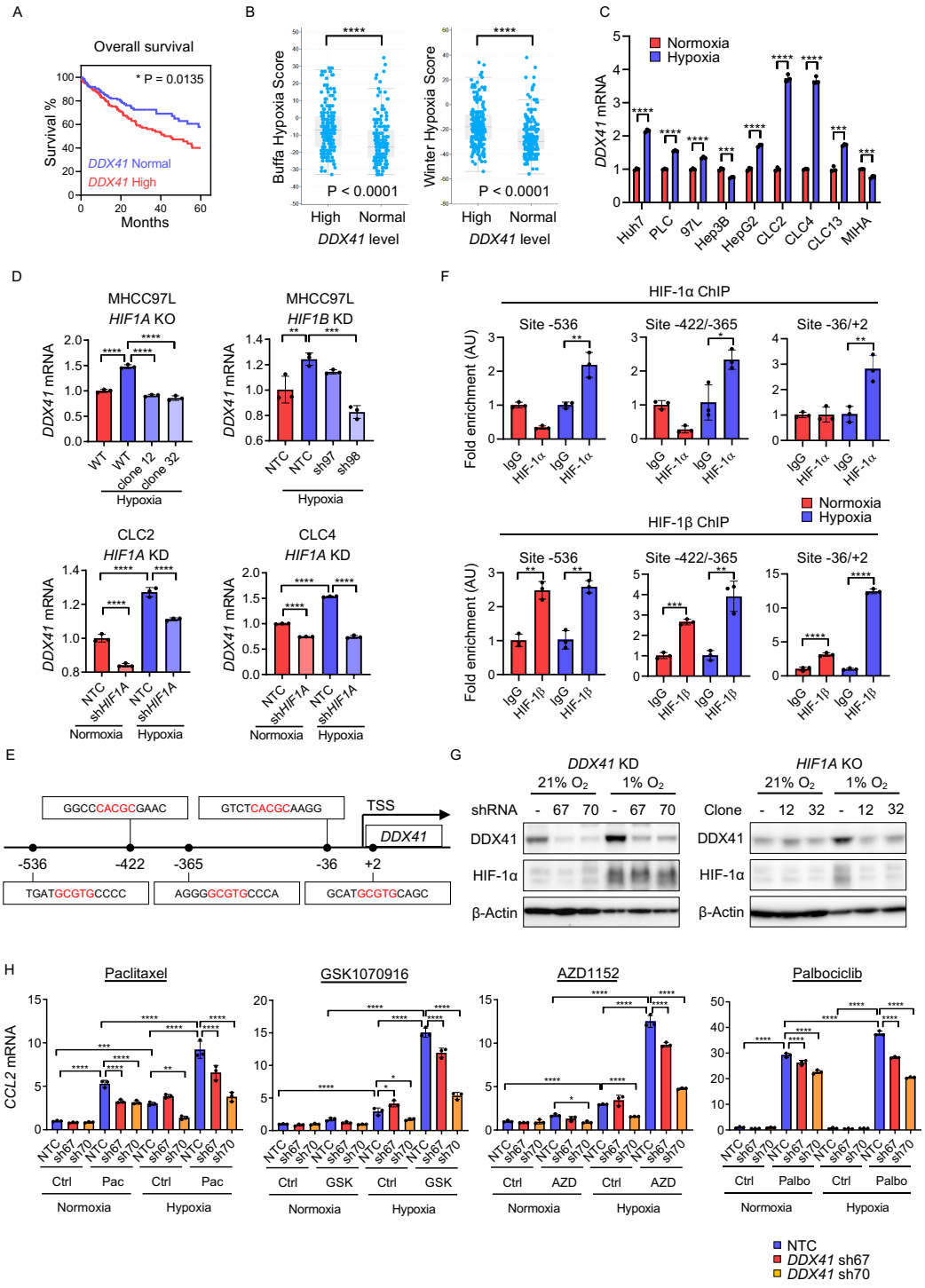

Figure 4. Hypoxia further exaggerated the effect of cell cycle inhibitors on SASP secretion via up-regulating DDX41

A. TCGA data showing the correlation between HCC patients with normal or high

expression level of *DDX41* and the percentage of survival in overall survival model (n=165 in DDX41 normal group; n=200 in DDX41 high group). The high *DDX41* expression level was defined as *DDX41* mRNA expression higher than the mean value (Z > 0). Log-rank (Mantel-Cox) test. **B.** TCGA data showing the Buffa hypoxia score and Winter hypoxia score of HCC patients with normal or high expression level of *DDX41*. Wilcoxon test. **C.** The HCC cells lines Huh7, PLC/PRF/5 (PLC), MHCC97L (97L), Hep3B, HepG2, CLC2, CLC4 and CLC13, and immortalized hepatocytes MIHA were exposed to normoxia with 21% O_2 or hypoxia with 1% O_2 for 24 hours. The cells were collected and RNA was extracted. The mRNA expression of *DDX41* was determined using RT-qPCR and normalized to housekeeping gene *18S*. *DDX41* expression in hypoxia was normalized to that in normoxia of the same cell line (n=3/group). **D.** *HIF1A* KO MHCC97L cells, *HIF1B* KD MHCC97L cells, *HIF1A* KD CLC2 cells and *HIF1A* KD CLC4 cells were exposed to normoxia with 21% O_2 or hypoxia with 1% O_2 for 24 hours. The mRNA expression of *DDX41* was determined using RT-qPCR and normalized to housekeeping gene *18S*. *DDX41* expression in hypoxia was normalized to that in wild type (WT) cells or NTC cells in normoxia (n=3/group). **E.** Diagram showing five putative hypoxia-response element (HRE) sites in the promotor region of *DDX41* where the transcription start site (TSS) is defined as 0. Red: HRE site. **F.** MHCC97L cells were exposed to normoxia with 21% O_2 or

hypoxia with 1% O_2 for 24 hours. The binding of HIF-1α or HIF-1β to the HRE sites of *DDX41* was detected using IgG, HIF-1α, or HIF-1β antibodies in chromatin immunoprecipitation (ChIP) assay. The enrichment of HIF-1α or HIF-1β was analyzed using qPCR with primers targeting different HRE sites in *DDX41* promotor. The fold of enrichment was determined by normalizing the enrichment level of HIF-1α, or HIF-1β to that of IgG (n=3/group). **G.** *DDX41* KD MHCC97L cells and *HIF1A* KO MHCC97L cells were exposed to normoxia with 21% O_2 or hypoxia with 1% O_2 for 24 hours. The cell lysate was extracted and western blot was used to show the protein expression level of DDX41 and HIF-1α, and β-actin was used as housekeeping protein. **H.** *DDX41* KD MHCC97L cells were treated with Paclitaxel, GSK1070916 or AZD1152 at the same time when exposed to normoxia with 21% O_2 or hypoxia with 1% O_2 for 48 hours. The cells were treated with Palbociclib for 24 hours first and were then exposed to normoxia or hypoxia for an addition of 48 hours. The RNA was extracted and mRNA expression of *CCL2* was determined using RT-qPCR. The *CCL2* expression level was normalized to that in control treatment in NTC cells in normoxia (n=3/group). Scatter dot plot: mean with SD. **A-C, F.** Student's t test. **D,H.** One-way ANOVA with Bonferroni Correction. * $P < 0.05$, ** $P < 0.01$, *** $P < 0.001$, **** $P < 0.0001$.

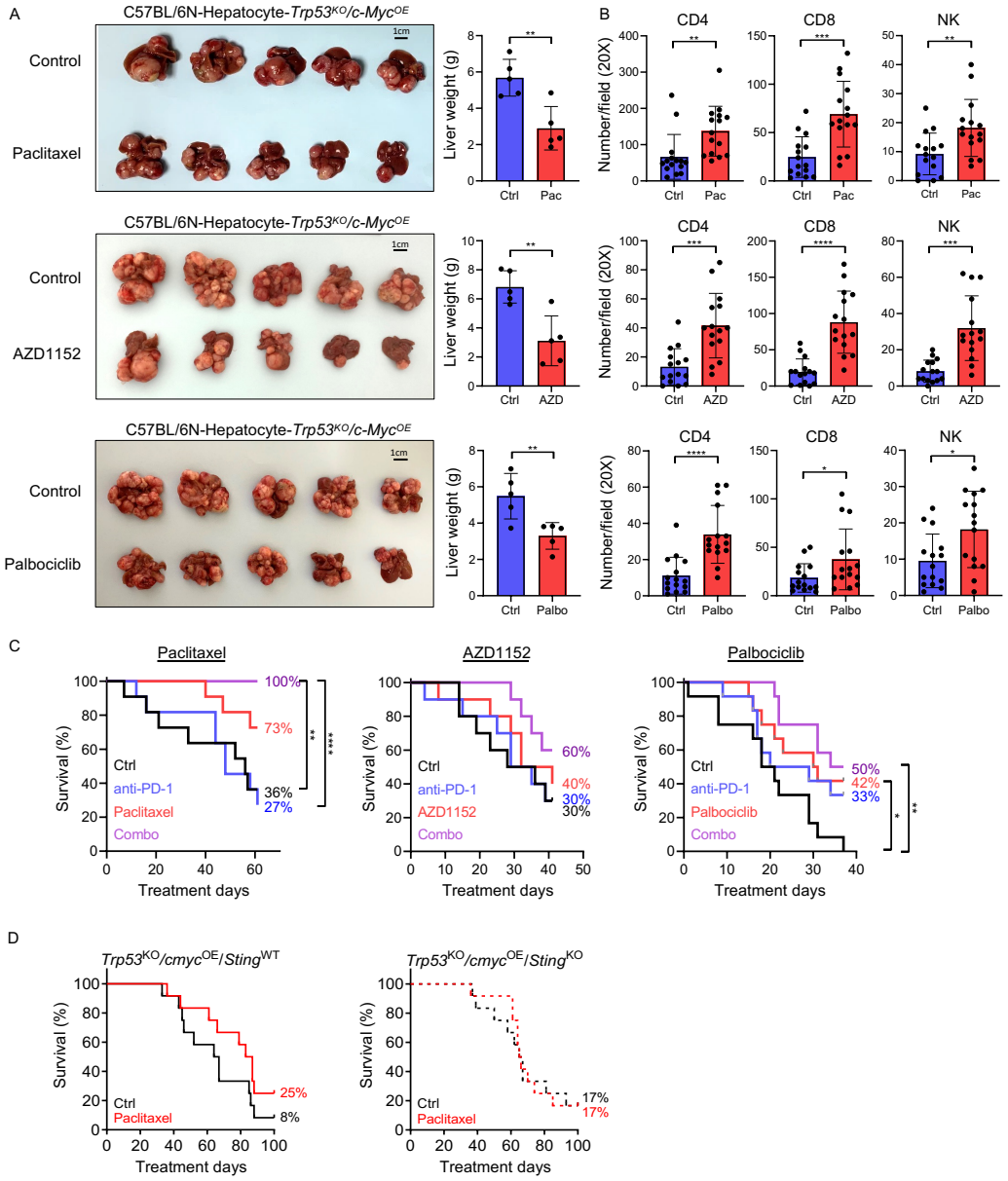

Figure 5. Cell cycle inhibitors induced immune surveillance in HCC tumors and promoted survival in combination with immune checkpoint inhibitor.

A - B. Cell cycle inhibitors were administrated to *Trp53*^{KO}/*c-Myc*^{OE} HCC tumor-bearing C57BL/6N mice three weeks after HDTVi. The tumors were harvested 28 days after Paclitaxel treatment, 20 days after AZD1152 treatment or 16 days after Palbociclib treatment (n=5 mice per group). **A.** Images showing the size and morphology of HCC tumors in control and cell cycle inhibitors-treated mice. Scale: 1 cm. The liver weight was measured. **B.** The tumors were fixed and prepared for paraffin-embedded slices (The plots were analyzed with 3 sections from each mouse, in total 15 sections from 5 mice). CD4 T cells, CD8 T cells and NK cells were detected using mouse CD4, CD8α and KLrb1c/CD161c antibodies in IHC staining. The numbers of CD4 T cells, CD8 T cells and NK cells were quantified per field in paraffin-embedded slices of control and cell cycle inhibitors-treated mice. Scatter dot plot: mean with SD. Student's t test. **C.** Vehicle control, cell cycle inhibitors alone, anti-PD-1 antibody alone or combined treatment of cell cycle inhibitors with anti-PD-1 antibody were administrated to *Trp53*^{KO}/*c-Myc*^{OE} HCC tumor-bearing C57BL/6N mice after HDTVi. Paclitaxel and anti-PD-1 antibody were administrated 19 days and 21 days after HDTVi respectively (n=11 mice/group). AZD1152 and anti-PD-1 antibody were administrated 16 days and 30 days after HDTVi respectively (n=10 mice/group). Palbociclib and anti-PD-1 antibody were administrated 18 days and 21 days after HDTVi respectively continuously (n=12 mice/group). **D.** Survival curves of *Sting* wildtype (WT) and *Sting*

knockout (KO) HCC bearing mice with vehicle control or Paclitaxel treatment administrated 22 days after HDTVi (n=12 mice/group). The percentage of survival mice was determined over treatment time. Log-rank (Mantel-Cox) test. * $P < 0.05$, ** $P < 0.01$, *** $P < 0.001$, **** $P < 0.0001$.

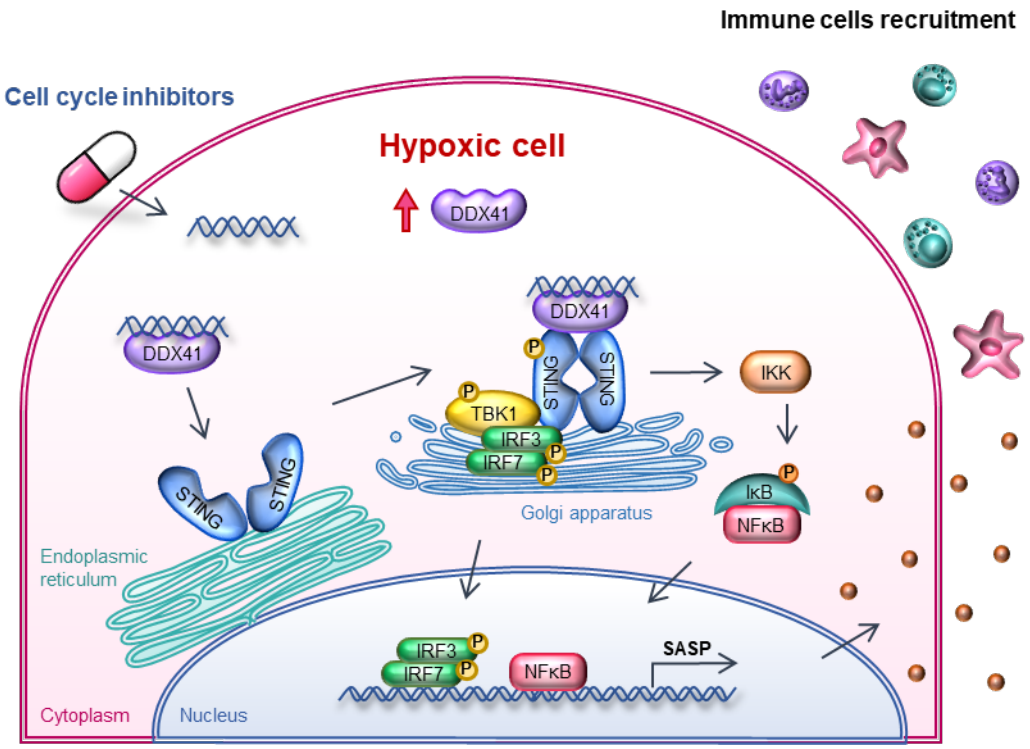

Figure 6. Research summary: Cell cycle inhibitors trigger immune response via DDX41-STING pathway

Schematic diagram showing the cell cycle inhibitors trigger immune response via DDX41-STING pathway. HCC tumor is highly hypoxic, which induces the upregulation of DDX41 expression in cells. Since both hypoxia and over-expression of DDX41 are detrimental to cell, cell cycle inhibitors are used to induce cytosolic DNA accumulation and trigger the activation of DDX41 as a cytosolic DNA sensor. The activated DDX41 binds to both the cytosolic DNA and STING. Upon activation, STING dimerizes and translocates from ER to Golgi apparatus and recruits TBK1. TBK1 auto-phosphorylates and further phosphorylates STING and facilitates the

recruitment and activation of IRF3 and IRF7. IRF3 and IRF7 form homodimer or heterodimer and translocate to nucleus for SASP expression. STING also activates IκB kinase (IKK) which then phosphorylates and inhibits the inhibitor of NFκB (IκB). Without the binding of IκB, the NFκB translocates to nucleus for SASP expression. The secreted SASPs recruit the infiltration of both innate and adaptive immune cells, especially NK cells, CD4 T cells and CD8 T cells to HCC tumor core for cancer clearance. The cytotoxic potential of those infiltrated immune cells can be further enhanced by using immune checkpoint inhibitors for example anti-PD-1 antibody, which suggests the potential of combined treatment of cell cycle inhibitors with immunotherapy.